HOLOGIC®
The Science of Sure

Powerful images.
Clear answers.

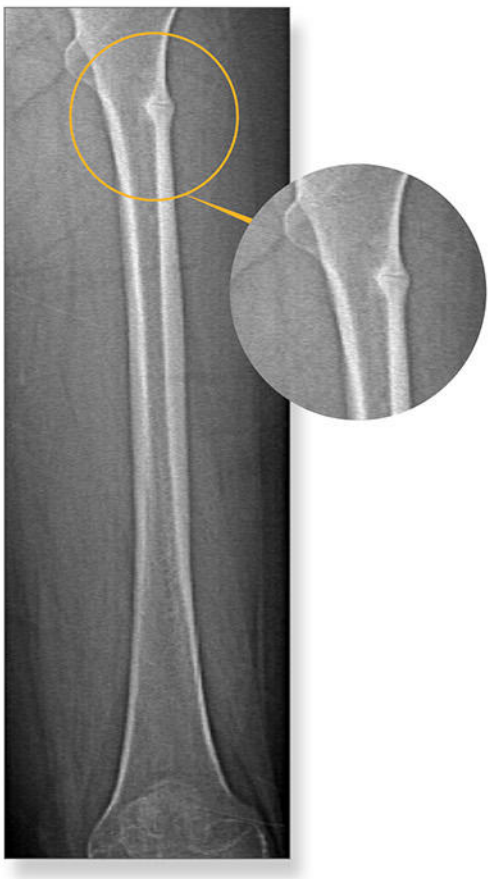

Manage Patient's concerns about Atypical Femur Fracture*

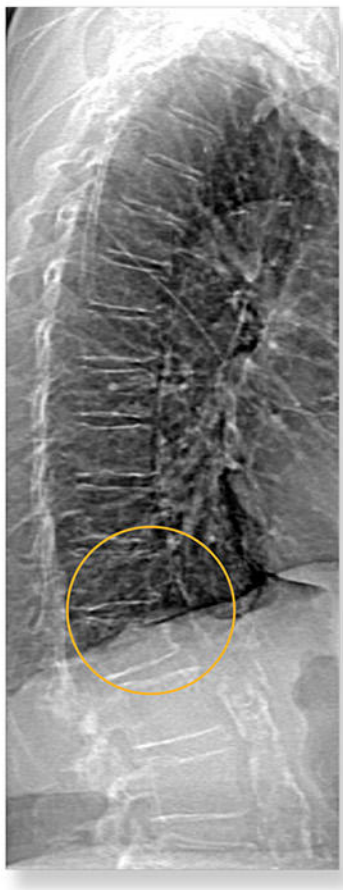

Vertebral Fracture Assessment – a critical part of a complete fracture risk assessment

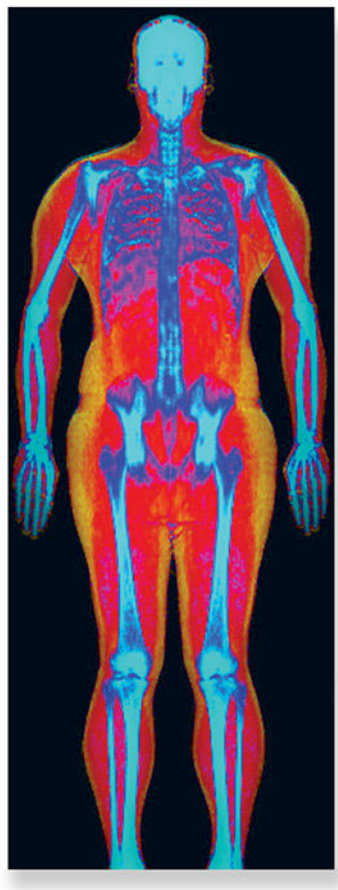

Advanced Body Composition® Assessment – the power to see what's inside

Contact your Hologic rep today at insidesales@hologic.com

*Incomplete Atypical Femur Fractures imaged with a Hologic densitometer, courtesy of Prof. Cheung, University of Toronto

www.hologic.com | info@hologic.com | 1.781.999.7300

ORIGINAL ARTICLE

JBMR®

Genetic and Molecular Insights Into Genotype-Phenotype Relationships in Osteopathia Striata With Cranial Sclerosis (OSCS) Through the Analysis of Novel Mouse Wtx Mutant Alleles

Glenda Comai,[1,2] Agnès Boutet,[1,3] Kristina Tanneberger,[4] Filippo Massa,[1] Ana-Sofia Rocha,[1] Aurelie Charlet,[1] Clara Panzolini,[1] Fariba Jian Motamedi,[1] Robert Brommage,[5] Wolfgang Hans,[5] Thomas Funck-Brentano,[6,7] Martin Hrabe de Angelis,[5,8,9] Christine Hartmann,[10] Martine Cohen-Solal,[6,7] Jürgen Behrens,[4] and Andreas Schedl[1]

[1]Université Côte d'Azur, INSERM, CNRS, Institut de Biologie Valrose (iBV), Nice, France
[2]Current Address: Dept. of Developmental & Stem Cell Biology, Pasteur Institute, CNRS UMR3738, Paris, France
[3]Current Address: CNRS, Sorbonne Université, UPMC Univ Paris 6, UMR8227, Translation, Cell Cycle and Development Group, Station Biologique, F-29688 Roscoff, France
[4]Friedrich-Alexander Universität Erlangen-Nuremberg, Nikolaus Fiebiger Zentrum, Erlangen, Germany
[5]German Mouse Clinic, Institute of Experimental Genetics, Helmholtz Zentrum München, German Research Center for Environmental Health, Neuherberg, Germany
[6]INSERM UMR-1132, Biologie de l'os et du cartilage (BIOSCAR), Paris, France
[7]Université Paris Diderot, Sorbonne Paris Cité, Paris, France
[8]Experimental Genetics, School of Life Science Weihenstephan, Technische Universität München, Freising, Germany
[9]German Center for Diabetes Research (DZD), Neuherberg, Germany
[10]Institute of Musculoskeletal Medicine, University Hospital Münster, Westfälische Wilhelms-Universität (WWU), Münster, Germany

ABSTRACT

The X-linked WTX/AMER1 protein constitutes an important component of the β-catenin destruction complex that can both enhance and suppress canonical β-catenin signaling. Somatic mutations in WTX/AMER1 have been found in a proportion of the pediatric kidney cancer Wilms' tumor. By contrast, germline mutations cause the severe sclerosing bone dysplasia osteopathia striata congenita with cranial sclerosis (OSCS), a condition usually associated with fetal or perinatal lethality in male patients. Here we address the developmental and molecular function of WTX by generating two novel mouse alleles. We show that in addition to the previously reported skeletal abnormalities, loss of *Wtx* causes severe midline fusion defects including cleft palate and ectopic synostosis at the base of the skull. By contrast, deletion of the C-terminal part of the protein results in only mild developmental abnormalities permitting survival beyond birth. Adult analysis, however, revealed skeletal defects including changed skull morphology and an increased whole-body bone density, resembling a subgroup of male patients carrying a milder, survivable phenotype. Molecular analysis in vitro showed that while β-catenin fails to co-immunoprecipitate with the truncated protein, partial recruitment appears to be achieved in an indirect manner using AXIN/AXIN2 as a molecular bridge. Taken together our analysis provides a novel model for WTX-caused bone diseases and explains on the molecular level how truncation mutations in this gene may retain some of WTX-protein functions. © 2018 American Society for Bone and Mineral Research.

KEY WORDS: BONE DEVELOPMENT; B-CATENIN SIGNALING; OSCS; MOUSE MODELS

Introduction

β-catenin is a multifunctional protein that plays important roles in cellular adhesion and as a signal transducer in the canonical Wnt signaling pathway.[1,2] Under normal conditions, free β-catenin quickly associates with AXIN, adenomatous polyposis coli (APC), and glycogen synthase kinase 3β (GSK3β) in a multiprotein complex. Phosphorylation of β-catenin by GSK3β

Received in original form June 30, 2017; revised form December 19, 2017; accepted January 3, 2018. Accepted manuscript online January 12, 2018.
correspondence to: Andreas Schedl, Institut de Biologie Valrose (iBV), Univ. Nice Sophia Antipolis, Centre de Biochimie; UFR Sciences; Parc Valrose, 28, avenue Valrose, 06108 Nice Cedex 2, France. E-mail: schedl@unice.fr
Additional Supporting Information may be found in the online version of this article.
Journal of Bone and Mineral Research, Vol. 33, No. 5, May 2018, pp 875–887
DOI: 10.1002/jbmr.3387

leads to its targeting to the proteasome pathway and its rapid degradation, thus keeping cytoplasmic β-catenin levels low. Binding of a WNT ligand to its receptors Frizzled (Fz) and the low-density lipoprotein receptor-related protein 5/6 (LRP5/6) results in recruitment of AXIN to the membrane and the disruption of the degradation complex. As a result, β-catenin is no longer phosphorylated, accumulates in the cell and translocates to the nucleus, where it interacts with DNA-binding proteins to regulate downstream effector genes.[3] Given its central role in the canonical Wnt signaling pathway, it is not surprising that loss-of-function mutations in β-catenin, or in one of its modulators, lead to serious developmental abnormalities in a wide variety of tissues.[1] Moreover, mutations that cause an increase in β-catenin levels are often associated with cancers[4] including the pediatric kidney cancer Wilms' tumor.[5]

WTX/AMER1 is X-chromosome–linked and has been identified as a gene carrying somatic mutations in a proportion of Wilms' tumors.[6] On a molecular level WTX appears to form part of the AXIN/APC/GSK3β multiprotein complex.[7–9] A series of experiments have demonstrated that WTX enhances β-catenin ubiquitination and degradation and therefore can act as a negative regulator of canonical WNT signaling.[8,9] In addition, molecular studies suggested that WTX also recruits GSK3β to the membrane, where it can stimulate LRP6 phosphorylation, at least in vitro.[10] Biochemical and cellular studies have revealed seven conserved residues in the N-terminus of WTX that are crucial for its binding to the plasma membrane[8] and four domains that confer binding to APC.[7,11] WTX also contains two regions capable of interacting with AXIN1/AXIN2.[8,10] On the other hand the C-terminal half of this protein was shown to directly bind to β-catenin.[8,9] This C-terminal domain was also suggested to mediate translocation of the WTX protein to the nucleus, where it can interact with the Wilms' tumor suppressor protein WT1, stimulate its activity as a transcriptional regulator in vitro,[12] and also act as a modulator of p53 function.[13]

Although somatic mutations in *WTX* are associated with Wilms' tumors, germline mutations in this gene instead cause the X-linked dominant congenital skeletal disease osteopathia striata congenita with cranial sclerosis (OSCS; OMIM 300373).[14,15] In heterozygous females, this condition is characterized by sclerosis of the long bones and skull, and longitudinal striations visible on radiographs in the metaphyseal regions of the long bones, pelvis, and scapulae. Other common clinical findings of OSCS include craniofacial malformations (macrocephaly, frontal bossing, ocular hypertelorism, broad nasal bridge), hearing loss, abnormalities of the palate, and mild learning difficulties.[14–16] Hemizygous mutations in males are typically associated with fetal or neonatal lethality due to an array of developmental malformations (ie, omphalocele, limb patterning, genitourinary and cardiac defects) besides the sclerotic bone phenotype.[14,17] However, there are subgroups of male patients which carry truncation mutations at or after the second APC binding domain that display a milder phenotype resembling those of heterozygous female patients and permit survival to adulthood.[14,17] The molecular explanation for these less severe phenotypes is unclear, but it has been speculated that these truncated proteins retain some functionality with the retention of the N-terminal WTX membrane interaction domain and at least one of the three APC binding sites.[14]

The Wnt/β-catenin signaling pathway has been shown to play key roles in bone formation and bone homeostasis in the adult. Consequently, mutations that affect β-catenin expression levels and β-catenin activity often result in skeletal defects.[18] Therefore, a role for WTX as a negative regulator of β-catenin stability fits well with the observed bone malformations in OSCS patients. Indeed, deletion of *Wtx* in mice leads to tissue overgrowth, increased bone density, and loss of adipose tissue.[19] On a molecular level this phenotype has been attributed to a role for WTX in controlling the switch of mesenchymal precursors between the adipocyte and osteoblast lineage through the regulation of β-catenin levels.

In the present study we further dissected the developmental and molecular function of WTX in vivo by generating a loss-of-function and a hypomorphic allele in the mouse. Consistent with earlier observations, complete loss of *Wtx* causes perinatal death and we describe a range of previously unreported severe midline skeletal defects. Surprisingly, deletion of the C-terminal half of *Wtx* ($Wtx^{flox\Delta}$ allele) is compatible with postnatal life and results only in relatively minor developmental bone patterning defects. Our in vitro data revealed that the truncated $WTX^{flox\Delta}$ protein can localize to the plasma membrane, and interact with β-catenin and GSK3β indirectly through its association with the scaffolding proteins AXIN1/AXIN2. Compensation, however, is incomplete and adult mice display skeletal dysplasia that recapitulates the phenotype found in human XY patients with 3′ deletions.

Materials and Methods

Mice

The targeting construct of the conditional *Wtx* allele was obtained by insertion of a first loxP into a ClaI site 333 bp upstream of the first ATG in exon2 and insertion of a floxed cassette containing a phosphoglycerate kinase I (PGK) promoter, neomycin resistance gene (NEO) and Herpes simplex virus-thymidine kinase (HSVtk) gene into a BamHI site 1674 bp downstream the first codon (Supplementary Fig. 1.A.a). Screening for positively targeted R1 embryonic stem (ES) cells[20] after Neomycin selection was first performed by nested PCR with Targ_fw/pflox225/Targ_fw2 primers (Supplementary Fig. 1.A.a). Positively targeted ES cells were confirmed by Southern blot using an external 3′ probe on PstI-digested genomic DNA (Supplementary Fig. 1B). The PGK-NEO/HSVtk cassette was removed in vitro by electroporation of targeted ES cells with a Cre recombinase expression vector and 1-(2-deoxy-2-fluoro-1-D-arabinofuranosyl)-5-iodouracil (fialuridine or FIAU) selection (Supplementary Fig. 1.A.b). Chimeric mice containing the $Wtx^{flox\Delta}$ allele were obtained by injection of $Wtx^{flox\Delta}$ ES cells into C57BL/6J mouse blastocysts. The Wtx^{KO} allele was obtained in vivo by germline deletion of the $Wtx^{flox\Delta}$ allele with the *Del-Cre*[21] or *Sox2-Cre*[22] lines (Supplementary Fig. 1.A.c). Routine genotyping was performed by PCR from earmarks or tail tips using the following primers: Primer_a: tggacgcaactcagagatgt and Primer_b: caactgcttctggatggtca for the flox allele, and Primer_c: ttggtcaggatggatgattg and Primer_b for the KO allele (Supplementary Fig. 1.A.b, 1.A.c, Supplementary Fig. 2.C). All genotyping PCR reactions were carried out in the GoTaq® Green Master Mix (Promega, San Luis Obispo, CA, USA).

Control and mutant mice were analyzed as littermates on a 129xC57Bl/6 hybrid background. All animal work was conducted according to national and international guidelines and was approved by the local ethics committee (PEA-NCE/2013-88). Animals were bred following the scheme on Supplementary Fig. 2A, B. The conditional *β-catenin* mouse line has been described.[23] Compound Wtx^{KO}; $\beta\text{-}catenin^{KO/+}$ embryos were generated by crossing *Del-Cre*$^{+}$ or *Sox2-Cre*$^{+}$ $\beta\text{-}catenin^{fl/+}$ males

with $Wtx^{KO/+}$ female mice. To obtain embryos at the desired developmental stages, young adult $Wtx^{flox\Delta/+}$ or $Wtx^{KO/+}$ females were mated overnight, and animals with a vaginal plug at noon of the next day were considered as embryonic day (E) 0.5. Pregnant females were euthanized by cervical dislocation.

Plasmid constructions

The mouse *Wtx* expression plasmid (GFP-Wtx) has been described elsewhere.[24] The expression construct for the $Wtx^{flox\Delta}$ allele (GFP-$Wtx^{flox\Delta}$) was generated by insertion of the BstXI-ScaI restriction fragment, flanking the loxP site of the targeting construct, into the Wtx wild-type expression plasmid cut with the same enzymes. pcDNA-Flag-Axin1 has been provided by A. Kikuch. pcDNA-Flag-Axin2 and pcDNA-Flag-GSK3β plasmids have been described.[25] The WT1 expression plasmid was generated by cloning the human WT1 coding sequence (NCBI Reference Sequence: NM_000378.4) into the pCDNA3.1 expression vector.

Cell culture and transient transfection

HEK293T and MCF-7 cells were cultured at 37°C with 5% CO_2 in Dulbecco's modified Eagle's medium (Gibco, Paisley, UK; 11960) supplemented with 10% fetal calf serum, 1% penicillin/streptomycin, and 2 mM glutamine (Gibco, Grand Island, NY, USA; 25030081). For transient transfections, HEK293T cells were transfected with Fugene HD (Roche Diagnostics, Mannheim, Germany) and MCF-7 cells with polyethyleneimine (PEI) or TransIT-TKO (Mirus, Madison, WI, USA) according to the manufacturer's instructions.

Western blotting and coimmunoprecipitation

For analysis of protein expression, HEK293T cells were washed in ice-cold PBS and treated with radioimmunoprecipitation assay (RIPA) lysis buffer containing a protease inhibitor cocktail (Roche) on ice for 1 hour before harvesting, sonication, and centrifugation at 13500g for 20 min to remove cell debris. Cell lysates were boiled for 5 min in a 2× SDS standard sample buffer before being separated by electrophoresis on SDS-polyacrylamide gels. Proteins were then transferred to polyvinylidene fluoride (PVDF) membrane (Bio-Rad Laboratories, Hercules, CA, USA). The membranes were blocked in PBS containing 5% nonfat dried milk for 3 hours at room temperature (RT) before addition of the primary antibody and incubation, with agitation at 4°C overnight. After multiple washes with PBS, the membrane was incubated for 1 hour in blocking buffer containing the appropriate HRP-conjugated secondary antibody (Promega).

Co-immunoprecipitation experiments were performed as described.[8] For WT1 co-immunoprecipitation Protein A/G Magnetic Beads (Pierce, Rockford, IL, USA) were used.

Antibodies

The rabbit polyclonal antibody against WTX/AMER1 has been described.[7] Commercial antibodies used in this study were as follows: chicken anti-GFP (Abcam, Cambridge, UK; ab13970), rabbit anti-GFP (Abcam; ab290), mouse anti-GFP (Roche; mixture of clones 7.1 and 13.1), mouse anti-GAPDH (Santa Cruz Biotechnology, Santa Cruz, CA, USA; sc-32233), mouse anti-β-catenin (BD Transduction Laboratories, Oxford, UK; clone 14), rabbit anti-Axin1 (Cell Signaling Technology, Beverly, MA, USA; C76H11), rabbit anti-Axin2 (Cell Signaling; 76G6), rabbit anti-Gsk3β (Cell Signaling; 9315), rabbit anti-Flag (Sigma-Aldrich, St. Louis, MO, USA; F7425), mouse anti-Flag (Sigma-Aldrich; F3165), mouse anti-WT1 (DAKO, Carpinteria, CA, USA; M3561). Secondary antibodies were purchased from Jackson Immunoresearch (Cambridgeshire, UK).

Immunofluorescence

Axin1, Axin2, and Gsk3β were detected by immunofluorescence in transfected cells using anti-Flag or anti-Gsk3β antibodies as described.[7] GFP-WTX and GFP-$WTX^{flox\Delta}$ fusion proteins were detected by direct visualization of GFP fluorescence or by GFP immunofluorescence. Cells were fixed 48 hours after transfection for 10 min in 4% PFA and permeabilized with 0.1% Triton for 10 min at RT. After 1 hour blocking at RT in DMEM/10% FCS, the cells were incubated 1 hour with primary antibodies at RT, washed in PBS three times for 5 min at RT and then incubated with secondary antibodies for 1 hour at RT in DMEM/10% FCS. Cells were washed in PBS, nuclei were stained with Hoechst (Invitrogen) and slides mounted with Mowiol. Photographs were taken as described in Grohmann and colleagues.[7]

Skeletal staining and histology

For the Alcian blue/Alizarin red staining of whole newborn skeletons, mice were euthanized, skinned, eviscerated, fixed in 95% ethanol, and stained according to McLeod.[26] Photographs were taken on Zeiss Axio Zoom.V16 (Zeiss, Jena, Germany) with Zen software. Alcian blue/eosin staining on tissue sections was performed as described in Lyashenko and colleagues.[27]

X-ray and DXA analysis and micro–computed tomography

Adult mice were killed at 14 weeks of age by cervical dislocation, frozen, thawed, eviscerated, skinned, and fixed in 70% ethanol. Littermates for analysis (coming from seven litters for $Wtx^{flox\Delta/+}$ males and seven litters for $Wtx^{KO/+}$ females) were housed together and the following X-ray, DXA, and micro–computed tomography (μCT) analysis were performed in a blinded manner.

Mouse radiographs and DXA scans were obtained with an UltraFocusDXA scanner (Faxitron Bioptics, Tucson, AZ, USA) using standard protocols. Eviscerated carcasses were decapitated, with heads scanned using X-ray energy of 25 keV and 0.4 mA current for 10 s (9 μm pixel dimension) for measurements of skull dimensions. DXA scans of the body (minus head) employed a pixel size of 16 μm. Bone mineral density (BMD) parameters included bone area and volumetric bone mass density (vBMD; BMD divided by the square root of bone area), which adjusts BMD values for bone size.[28] Femurs and tibia were dissected from the carcasses and lengths measured with Vernier calipers. Spine lengths were measured from radiographs. μCT analyses involved the use of a SKYSCAN 1272 scanner (Bruker, Coventry, UK). Bones were placed vertically and scanned with the settings: aluminum filter, 0.5 mm; resolution, 6 μm; energy, 70 to 90 kV; intensity, 100 μA; and integration time, 170 ms. Reconstruction of femurs and analysis of bone volume involved the use of CT analyzer. The histomorphometric variables were expressed in compliance with the recommendation of the ASBMR Histomorphometry Nomenclature Committee.[29]

RNA assays

Total RNA from homogenized E11.5 embryos was isolated with the RNeasy Mini kit (QIAGEN, Valencia, CA, USA) following the

manufacturer's instructions. cDNA was synthesized using a Superscript III first-strand cDNA synthesis kit (Invitrogen). *Wtx* relative expression levels were calculated as the ratio of the absolute quantifications, obtained by the standard curve method, between *Wtx* and the housekeeping gene *Hprt*. (Hprtp95_fw: tcctcctcagaccgctttt, Hprtp95_rs: ctggttcatcatcgctaatc; Wtxp84_fw: cagaggctccagctcaaatc, Wtxp84_rs: gcatcacagtggggtcct) using the LightCycler® TaqMan® Master system (Roche Applied Science).

Statistics

The number of embryos/adult animals for the different analysis are reported in the corresponding Results section. Statistical analyses were performed using the GraphPad Prism v6 software (GraphPad Software, Inc., La Jolla, CA, USA). Statistical significance was assessed by the Mann-Whitney test or two-tailed Student's *t* test.

Results

Generation of two *Wtx* mutant alleles to study the in vivo role of WTX

To address the in vivo function of the C-terminal part of *WTX* and at the same time allow the generation of a loss-of-function allele, we inserted *loxP* sites upstream of exon 2 and at nucleotide position 1674 of the coding region (NCBI Reference Sequence: NP_780388.2) (Fig. 1*A*, Supplementary Fig. 1A, B). The presence of two stop codons within the *loxP* cassette is expected to lead to a truncated WTX$^{flox\Delta}$ protein that maintains the highly conserved N-terminal region, which is required for the interaction with APC and recruitment to the plasma membrane.[7,8] However, the truncated protein lacks the C-terminal domain that is required for the interaction with β-catenin, WT1, and appears to be necessary for nuclear localization.[8,12] The second allele (*Wtx*^{KO}) was generated by Cre-mediated deletion of the *loxP* flanked sequences using a ubiquitously active Cre deleter (*Del-Cre*[21]) or an epiblast specific deleter strain (*Sox2-Cre*[22]). The *Wtx*^{KO} allele lacks the entire N-terminus of *Wtx* including splice acceptor regions and translation start site and thus should represent a null allele (Fig. 1*A*, Supplementary Fig. 1A). RT-PCR analysis on RNA isolated from E11.5 embryos showed normal splicing of the targeted allele in *Wtx*$^{flox\Delta}$, but failed to amplify a specific band in *Wtx*^{KO} mice, demonstrating that no *Wtx* transcript is produced from the KO allele (Supplementary Fig. 1C). Similarly, no amplification was observed by qRT-PCR with both a 5′ intron spanning and 3′ non-intron spanning primer sets on E13.5 embryos (Supplementary Fig. 1D and data not shown).

To evaluate the molecular properties of the truncated WTX$^{flox\Delta}$ protein we generated expression plasmids that mimic the *Wtx* wild-type and *Wtx*$^{flox\Delta}$ alleles, but carry a GFP-reporter fused to their N-terminal end. Western blotting with antibodies against GFP or WTX confirmed the presence of the predicted 217-kDa and the 115-kDa truncated protein in *GFP-Wtx* and *GFP-Wtx*$^{flox\Delta}$ transfected HEK293 cells, respectively (Supplementary Fig. 1E). Analysis at the subcellular level revealed that GFP-WTX localized within the cytoplasm, at the plasma membrane and in 16% of the cells in a speckled pattern within the nucleus, representing paraspeckles, as reported previously.[12] The truncated GFP-WTX$^{flox\Delta}$ protein maintained staining at the plasma membrane and to a lesser extent in the cytoplasm but showed reduced nuclear localization (Fig. 1*B*). These findings are consistent with the loss of the C-terminal nuclear translocation domain in the truncated GFP-WTX$^{flox\Delta}$ protein.[12] Pull-down experiments further demonstrated that the truncated protein was no longer able to interact with either of the two main alternatively spliced isoforms (+KTS and –KTS) of the Wilms' tumor suppressor WT1 (Fig. 1*C*).

WTX can also directly interact with β-catenin and co-immunoprecipitation experiments in transfected HEK293 cells confirmed this interaction for the GFP-WTX protein (Fig. 1*D*). By contrast, assays with the GFP-WTX$^{flox\Delta}$ plasmid showed that the truncated protein fails to precipitate co-transfected β-catenin, thus corroborating earlier findings that demonstrated a requirement of the C-terminal region of WTX for direct binding.[8,9]

Taken together, these data indicate that *GFP-Wtx*$^{flox\Delta}$ results in a shorter protein that fails to enter the nucleus and cannot longer interact with WT1 or β-catenin.

Calvarial and midline developmental defects in *Wtx* mutant alleles

We next addressed the in vivo function of the newly generated alleles (Supplementary Fig. 2A–C). Both *Wtx*^{KO} and *Wtx*$^{flox\Delta}$ animals were born at the expected Mendelian rates (Supplementary Fig. 2D, E). As reported,[19] *Wtx*^{KO} males (XY *Wtx*^{KO}) died soon after birth and displayed somatic overgrowth and increased body mass compared to controls (Fig. 2*A*, *B*; Supplementary Fig. 2F). By contrast, *Wtx*$^{flox\Delta}$ males were viable, fertile, and produced offspring (Fig. 2*B*; Supplementary Fig. 2G), demonstrating that deletion of the C-terminal half of *Wtx* (*Wtx*$^{flox\Delta}$ allele) was compatible with postnatal life.

During development, *Wtx* is expressed in the metanephric mesenchyme surrounding the branching epithelium,[6,30] and thus would be active in the progenitor cell population that is supposed to give rise to Wilms' tumor. We did not observe the development of kidney tumors in *Wtx*$^{flox\Delta}$ or *Wtx*$^{KO/+}$ adult mice, but inspection of the urogenital region between E13.5 and birth revealed unilateral or bilateral renal agenesis in up to 62% of *Wtx*^{KO} mice analyzed (Supplementary Fig. 2I). As reported,[19] this phenotype appeared to be genetic background–dependent. Kidney development in *Wtx*$^{flox\Delta}$ mutants was indistinguishable from wild-type littermates (data not shown).

To further assess the importance of the C-terminal domain of WTX during skeletal development, we decided to perform a detailed comparison between our *Wtx*^{KO} and *Wtx*$^{flox\Delta}$ alleles. Because WTX is an X-linked gene for which males are constitutively hemizygous, we focused our developmental analysis on male mice, thus limiting the inherent variability observed in heterozygote females due to differences in X-inactivation ratios. Close examination of *Wtx*^{KO} skulls at birth revealed a number of skeletal developmental defects including the presence of a complete cleft palate in 43% of the mutants (Fig. 2*C*; Supplementary Fig. 2J). Because cleft palate is incompatible with the survival of newborn mice, this could explain in part the cyanosis, lack of milk in the stomach, and perinatal lethality in 100% of *Wtx*^{KO} mice ($n = 58$, Fig. 2*B*). In addition, *Wtx*^{KO} mice showed an overall shortening of the skull and an increase in the width to length skull ratio (Fig. 2*D*, *E*). To evaluate whether the altered skull proportions maybe due to premature ossification of skull bones, we isolated calvarial osteoblasts from postnatal day 0 (P0) pups and analyzed their differentiation potential in vitro. Surprisingly, *Wtx* knockout osteoblasts showed a significant decrease rather than an

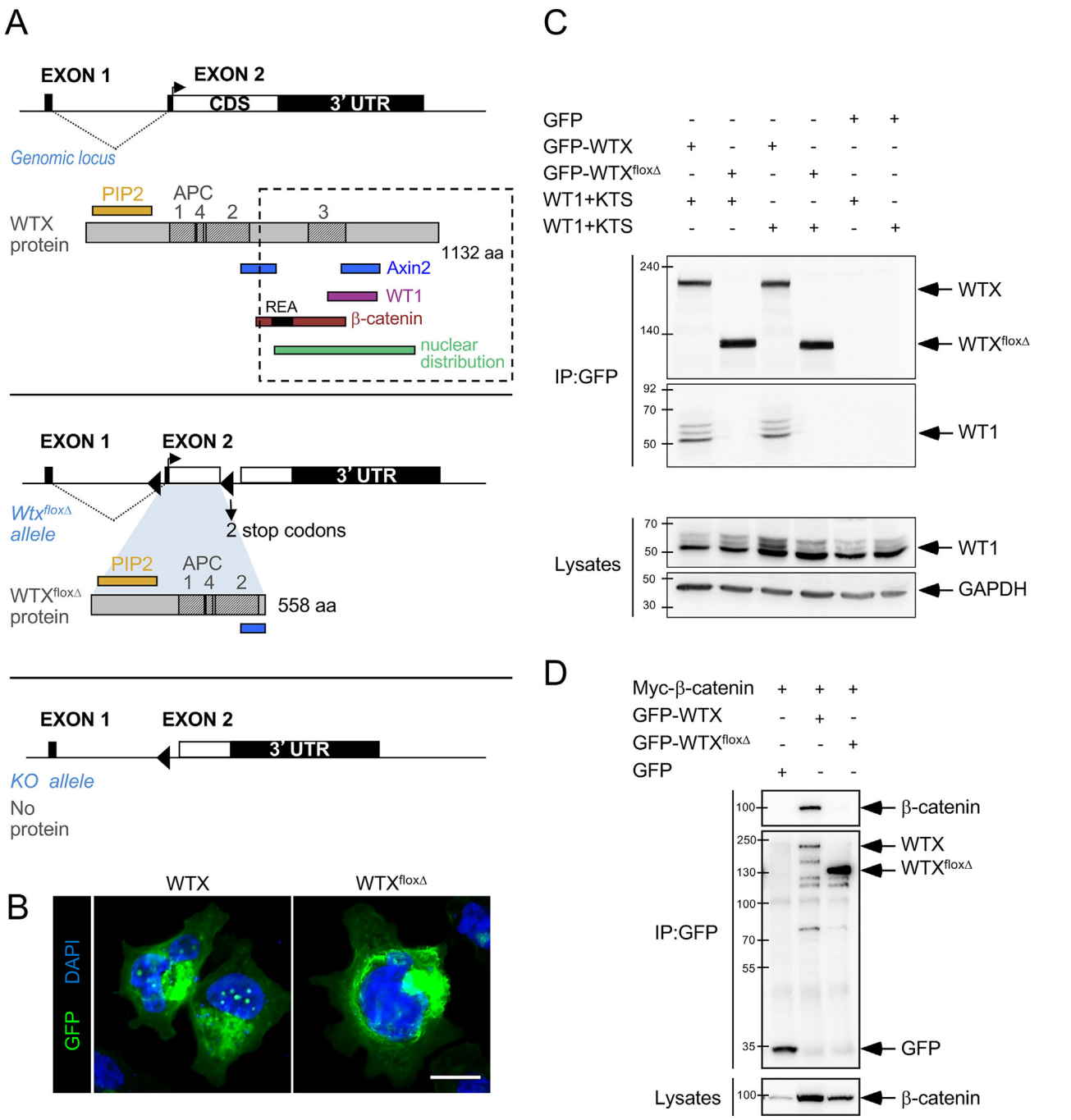

Fig. 1. Design and molecular characterization of novel *Wtx* mutant alleles. (*A*) Schematic drawing of the targeting strategy. White and black boxes signify CDS and UTRs, respectively. The domains previously described to be required for the interaction of WTX with APC (dashed boxes, APC1, APC4, APC2, APC3), Axin2 (conductin), WT1, β-catenin via the REA repeats, PIP2, and the region required for the nuclear localization are shown.[7–9,11,12] For the generation of the $Wtx^{flox\Delta}$ allele, loxP sites were inserted into intron 1 and within the coding region of exon2 (nucleotide position 1674). This results in the production of a shorter protein of 558 amino acids due to the presence of two stop codons. Recombination between the loxP sites by Cre recombinase leads to a Wtx^{KO} allele where no functional protein is produced. (*B*) Immunostaining of HEK293 transfected cells reveals that wild-type GFP-WTX is found at the plasma membrane, within the cytoplasm and in 16% of cells in a speckled pattern within the nucleus. The shorter GFP-$WTX^{flox\Delta}$ protein maintained staining at the plasma membrane and the cytoplasm, but showed reduced nuclear localization (4% of cells). Quantification was done on three independent transfection experiments ($n \geq 85$ cells). Scale bar = 10 μm. (*C*) Co-transfection experiments followed by Co-IP analysis reveal that in contrast to GFP-WTX, GFP-$WTX^{flox\Delta}$ is no longer able to interact efficiently with WT1+KTS and WT1-KTS. (*D*) GFP-WTX, but not GFP-$WTX^{flox\Delta}$ is able to co-immunoprecipitate with β-catenin. Numbers on the left of the images in *C* and *D* indicate positions of molecular weight markers (kD). CDS = coding region; UTR = untranslated region; PIP2 = phosphatidylinositol diphosphate; IP = co-immunoprecipitation.

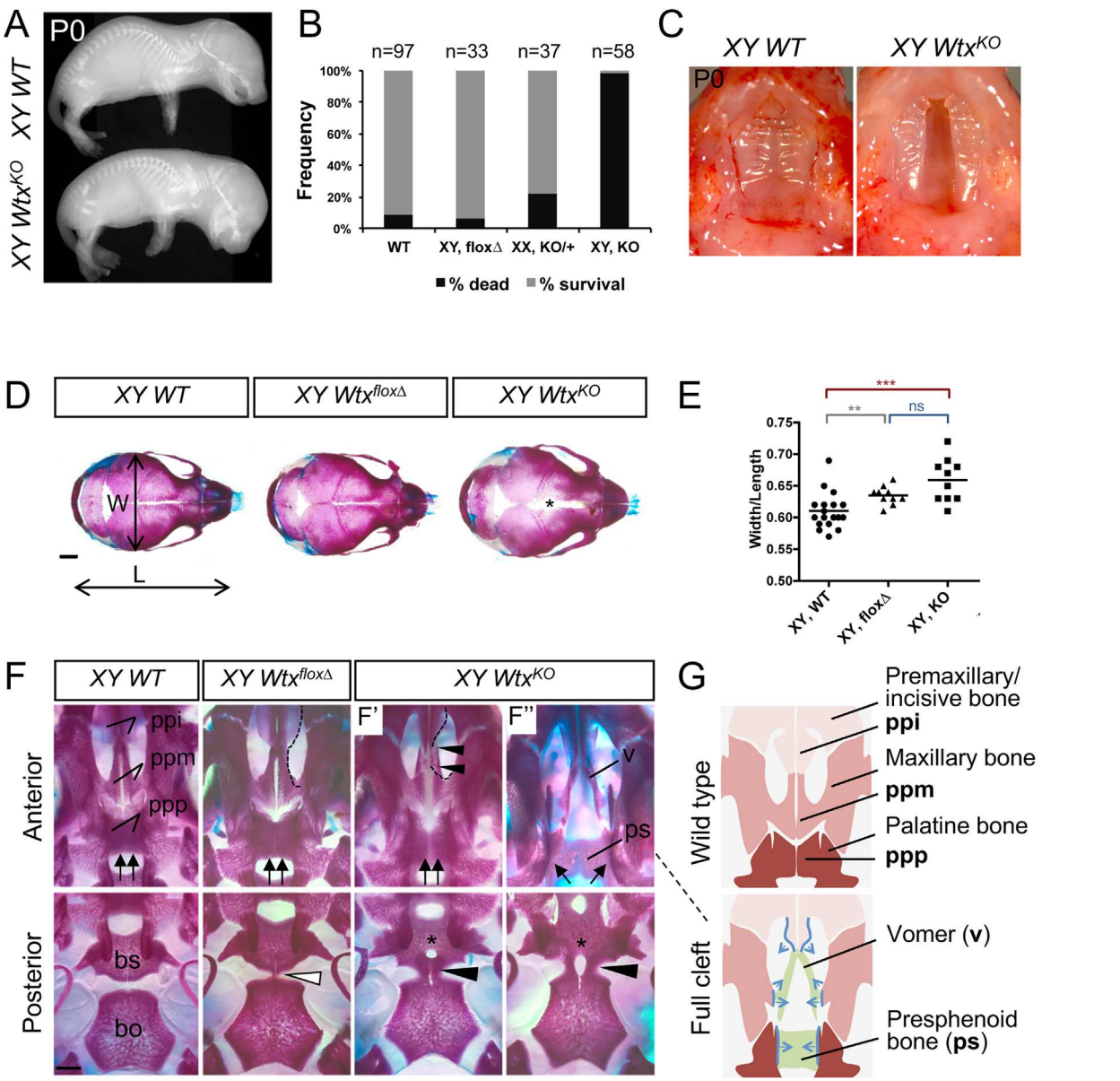

Fig. 2. Characterization of $Wtx^{floxΔ}$ and Wtx^{KO} alleles at birth. (*A*) X-ray analysis of P0 pups demonstrates a rounder shape of the skull and bigger size of Wtx^{KO} neonates. (*B*) Frequency of perinatal death on the indicated genotypes. (*C*) Ventral view of dissected newborn heads show a full cleft of the secondary palate in 43% of Wtx^{KO} embryos ($n = 16$). (*D*) Alizarin red/Alcian blue–stained skeletal preparations at P0. Top view of the skull reveals wide cranial fontanelles (asterisk) and increased width (W) to length (L) ratio in Wtx^{KO} embryos. $Wtx^{floxΔ}$ embryos show less marked altered cranial proportions. (*E*) Scatter plot showing the distribution (and mean) of the measurements in *D*. Mann-Whitney test: $^{**}p < 0.01$; $^{***}p < 0.001$; ns, nonsignificant. (*F*) Inferior views of skull base after removal of the mandible. Two different Wtx^{KO} embryos are included to show variability of the phenotype (*F′*, *F″*). Anterior view shows lack of fusion between the palatal processes of the maxillary and premaxillary/incisive bones (black arrowheads in *F′*). In cases of complete cleft of the secondary palate (*F″*), the palatal processes of the maxillary and palatine bones are severely hypoplastic or absent thus exposing the vomer and presphenoid. Small vertical arrows highlight convergence or not of the palatal processes of the palatine at the midline. Posterior view shows the presence of a thin bony bridge between the basisphenoid and basioccipital bone in 30% of $Wtx^{floxΔ}$ embryos (white arrowhead). A thicker bridge (black arrowhead) and a hole in the basisphenoid bone or through the bridge (asterisks in *F′*, *F″*) were present in 100% of Wtx^{KO} embryos (see Supplementary Table 1). (*G*) Schematic representations of a control and complete cleft palate situation. The bone processes that fail to grow medially and anterior-posteriorly to converge at the midline in the full cleft condition are outlined in blue. Adapted from Vanhoutteghem and colleagues.[59] *n* value ≥10 for all genotypes. Scale bars: *D* = 1000 μm; *F* = 500 μm. bs = basisphenoid, bo = basioccipital, ps = presphenoid, v = vomer, ppi = palatal process of premaxillary/incisive bone, ppm = palatal process of maxillary bone, ppp = palatal process of palatine; P0 = postnatal day 0.

increase in the formation of Alizarin red–stained bone nodules, thus excluding premature ossification as an explanation for the observed phenotype (Supplementary Fig. 2K). However, further inspection of the base of the skulls revealed a bony bridge connecting the basioccipital with the basisphenoid bone, which could explain the altered skull proportions observed in Wtx^{KO} mice (Fig. 2*F*). This phenotype was accompanied by the presence of a hole or cleft in the posterior region of the

basisphenoid bone in more than 90% of the mutants analyzed ($n = 13$) (Fig. 2*F*). Finally, examination of the base of the skull also helped us distinguish palatal clefts of different severity not detected by visual inspection of the oral cavity at birth. In the less severe cases, the palatal processes of the incisive and maxillary bones failed to extend and juxtapose at the midline (Fig. 2*F′*). In cases of a full cleft, the palatal processes of the maxillary and palatine bones were severely hypoplastic and allowed visualization of the presphenoid and vomer bones (Fig. 2*F″*, *G*). In contrast, $Wtx^{flox\Delta}$ mice displayed normal palate development and a very mild skull phenotype. Only 30% of $Wtx^{flox\Delta}$ mice ($n = 10$) presented a thin bony bridge connecting the basioccipital with the basisphenoid bones (Fig. 2*F*), probably explaining the less severe increase in the skull proportions (3%), when compared to the increase of Wtx^{KO} animals (8%) versus wild-type controls (Fig. 2*D*, *E*).

Examination of the remaining skeleton confirmed previous observations and revealed a number of additional skeletal defects (Supplementary Table 1). Wtx^{KO} pups presented a reduced or absent deltoid tuberosity (100%; Fig. 3*A*), split lumbar vertebral bodies (61%; Fig. 3*B*), and a pronounced alteration in spine curvature at the cervical level (100%; Supplementary Fig. 2L). All Wtx^{KO} pups analyzed ($n = 13$) displayed a split sternum, where the sternal bars were not fused at the midline (100%; Fig. 3*C*). The xiphoid process of the developing sternum was also abnormally bifurcated with two separate ossification centers remaining in some Wtx^{KO} pups. $Wtx^{flox\Delta}$ mice did not present these abnormalities, but displayed more subtle patterning defects ($n = 10$). The deltoid tuberosity was present, but appeared misshapen in $Wtx^{flox\Delta}$ mice (Fig. 3*A*). At the level of the developing sternum, fusion of the lower part of the sternal bars seemed to be delayed and fusion of the xiphoid process was incomplete in 30% of the $Wtx^{flox\Delta}$ mice analyzed (Fig. 3*C*). Finally, measurements along the anterior-posterior axis revealed that Wtx^{KO} mutant sternums were shortened, with the length of the ossified part of the manubrium being most severely affected (Fig. 3*D*). However, no significant change was found in $Wtx^{flox\Delta}$ mice. Overall, our phenotypic comparison during development at all anatomical locations between our two WTX alleles reveal a milder phenotype when the truncated $WTX^{flox\Delta}$ protein is present.

The $WTX^{flox\Delta}$ protein is able to interact indirectly with β-catenin via Axin

To address whether the skeletal defects described above were due to dysregulated β-catenin levels, we attempted to complement our complete *Wtx* mutants with a *β-catenin* loss-of-function allele.[23] Reduction in β-catenin gene dosage, partially rescued survival at P0 (Supplementary Fig. 3A; 58% survival, $n = 12$), and improved the calvarial proportions and sternal fusion defects due to *Wtx* deficiency (Supplementary Fig. 3B, C). Therefore, this result confirmed the previous observations[19] indicating that the relative abundance of these two proteins has to be tightly balanced during skeletal development. On this basis, the less severe phenotype in XY $Wtx^{flox\Delta}$ animals, when compared to a complete knockout (XY Wtx^{KO}), was surprising given the proposed function of WTX as a negative regulator of β-catenin and the fact that the truncated WTX protein is unable to directly bind β-catenin (Fig. 1*D*). Therefore, we decided to perform additional molecular analyses of the $WTX^{flox\Delta}$ protein. Previous in vitro studies suggested that WTX may exert its function by interacting with β-catenin and GSK3β indirectly through its association with the scaffolding proteins of the β-catenin degradation complex AXIN1/AXIN2.[10] To test whether the $WTX^{flox\Delta}$ protein was still able to bind to these proteins, we performed co-transfection assays in HEK293 cells. In this setting, both WTX and $WTX^{flox\Delta}$ were able to interact with overexpressed AXIN2 as demonstrated by co-immunoprecipitation experiments. In addition, both proteins were able to pull-down endogenous GSK3β and β-catenin in the presence of overexpressed AXIN1 or AXIN2 (Fig. 4*A*; Supplementary Fig. 4A; and data not shown). We could confirm these results by immunofluorescent microscopy on transfected MCF7 cells. $WTX^{flox\Delta}$ protein was still able to recruit both AXIN1 and AXIN2 to the cell membrane (Fig. 4*B*; Supplementary Fig. 4B). Similarly, the $WTX^{flox\Delta}$ protein was able to relocate GSK3β from its diffuse cytoplasmic localization to the membrane in the presence, but not in the absence of overexpressed AXIN2 (Fig. 4*C*, *D*). However, close inspection suggested that the recruitment of AXIN1 from its characteristic cytoplasmic puncta[31] by $WTX^{flox\Delta}$ protein was slightly less efficient when compared to wild-type WTX (Fig. 4*D*; Supplementary Fig. 4B). We conclude that the C-terminal domain of WTX is dispensable for survival and that—at least in vitro—the truncated $WTX^{flox\Delta}$ protein is still able to indirectly interact with β-catenin and recruit GSK3β to the membrane via its interaction with AXIN1/2, albeit in a slightly less efficient manner.

Truncation mutations cause increased bone mass density as observed in human patients

Survival of XY $Wtx^{flox\Delta}$ mice beyond birth (Supplementary Fig. 2G) permitted us to examine the effect of C-terminal truncations on bone development in adults (14 weeks). For comparison, we also analyzed XX $Wtx^{KO/+}$mice, which generally showed a more variable phenotype with a proportion of mice dying at birth (21.6%, $n = 37$; Fig. 2*B*). This variability is probably due to the stochastic nature of X-inactivation, which in certain $Wtx^{KO/+}$ embryos may result in the predominant inactivation of the wild-type *Wtx* allele, thus leading to an effective null phenotype and perinatal death. However, most heterozygote $Wtx^{KO/+}$ females were viable, fertile (Supplementary Fig. 2H), and could be used in the analysis. No significant differences in body weight were observed between either XY $Wtx^{flox\Delta}$ or XX $Wtx^{KO/+}$ mice and their respective littermate controls (Supplementary Fig. 5A).

Surviving $Wtx^{KO/+}$ females and some $Wtx^{flox\Delta}$ males displayed a noticeable shortening and dome-shaped appearance of the head that was more severe in the case of mutant females (Fig. 5*A*, *B*; and data not shown). This morphological feature permitted an easy identification of the *Wtx* heterozygous females among their wild-type littermates within the first 3 weeks after birth. Measurements of skulls after X-ray analysis revealed a significant increase in the width/length ratio in both XY $Wtx^{flox\Delta}$ (11%; $n = 11$) and XX $Wtx^{KO/+}$ (18%; $n = 12$) over control animals (Fig. 5*C*; Supplementary Fig. 5B, C). The altered skull architecture in mutant mice appeared to affect all bones proportionally, because no incisor malocclusions were observed.

No bone striations similar to those found in OSCS patients were observed in radiographs of spine, femur, or tibia of $Wtx^{KO/+}$ females (Supplementary Fig. 5D and data not shown). In addition, analysis of femur, tibia, and spinal column showed no significant length changes in XY $Wtx^{flox\Delta}$ and XX $Wtx^{KO/+}$ animals when compared to controls (Supplementary Fig. 5E). However, DXA scans revealed similar elevations of vBMD in the whole body of $Wtx^{flox\Delta}$ male (+8%) and $Wtx^{KO/+}$ female mice (+7%) (Fig. 5*D*).

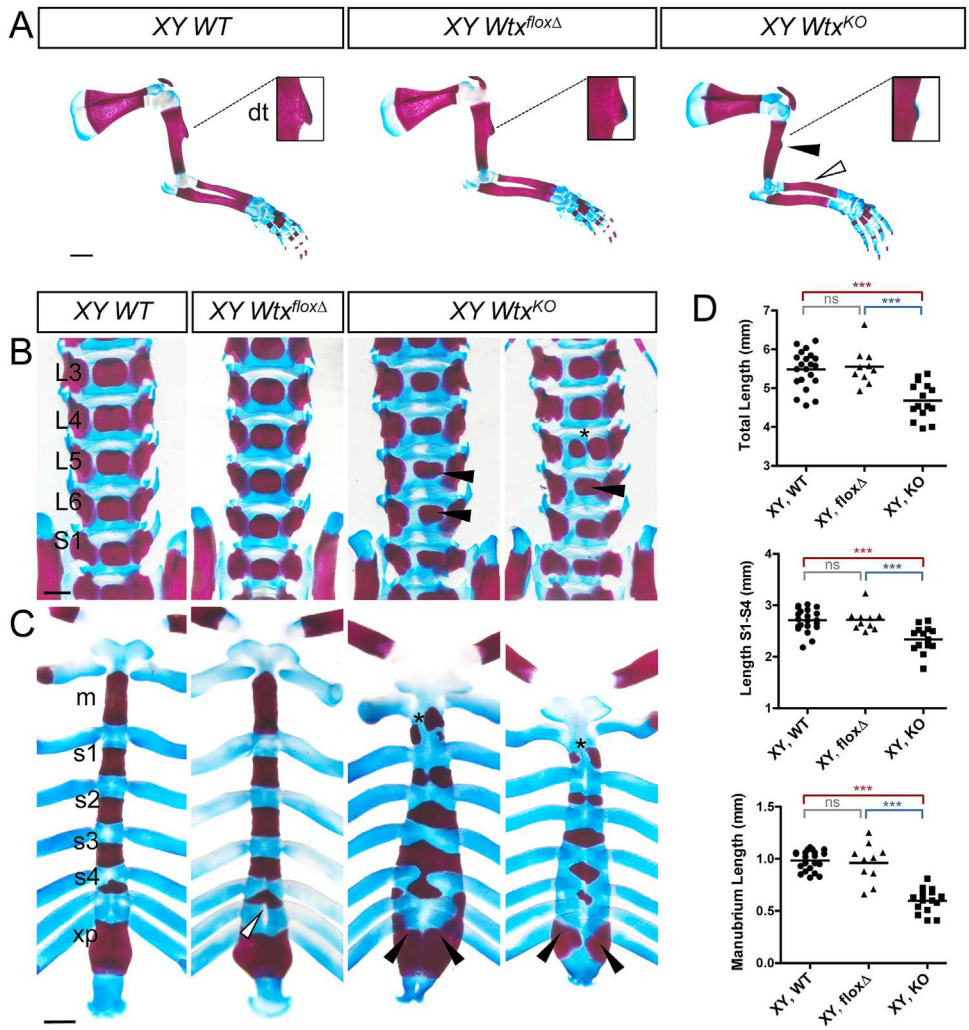

Fig. 3. Skeletal abnormalities of $Wtx^{floxΔ}$ and Wtx^{KO} alleles at birth. Alizarin red/Alcian blue–stained skeletal preparations at P0 reveal skeletal patterning and fusion defects in Wtx^{KO} embryos. (*A*) Reduction or absence of the deltoid tuberosity (dt, black arrowhead) and thickened radius (white arrowhead) in Wtx^{KO} embryos. (*B*) Occasional lack of fusion of lumbar vertebral bodies along the midline (asterisk) in Wtx^{KO} embryos. Vertebral bodies are often misshapen in the mutant (black arrowheads). Two different Wtx^{KO} embryos are shown to highlight variability of the phenotype. (*C*) Aberrant fusion of mutant sternebrae and xiphoid process leading to bifid sterna (black arrowheads). An asterisk in the anterior sternum depicts the presence of a stripe of cartilage in between the sternal bars of Wtx^{KO} embryos. In $Wtx^{floxΔ}$ embryos fusion in the lower part of the sternum is often delayed (white arrowhead). (*D*) Scatter plot showing the distribution (and mean) of individual sternal measurements. Total length refers to the distance between the uppermost ossified part of the manubrium and the lowermost ossified part of the xiphoid process. Length of manubrium refers to the length of the ossified part and distance s1 to s4 refers to the distance between the uppermost part of the ossification center s1 to the lowermost part of the ossification center s4 (Mann-Whitney test: $^{***}p < 0.001$; ns, nonsignificant). *n* value ≥10 for all genotypes. Scale bars: *A* = 1000 μm; *B*, *C* = 500 μm. P0 = postnatal day 0; m = manubrium, s1–s4 = sternebrae, xp = xiphoid process; L_3–L_6 = lumbar vertebrae; S1 = sacral vertebrae.

To analyze the bone phenotype further, we carried out μCT at the level of the distal femoral metaphysis. A small, but significant increase in trabecular bone volume to total bone volume ratio (BV/TV) was observed at the femur of $Wtx^{floxΔ}$ male mice (+4.5%) (Fig. 5*E*). The BV/TV of $Wtx^{KO/+}$ female mice at the femur levels was not significantly different from WT values, probably due to the higher phenotypic variability due to X-inactivation in females. The cortical and trabecular thickness did not exhibit statistically significant alterations in neither $Wtx^{floxΔ}$ male or $Wtx^{KO/+}$ female mice compared to controls. However, truncation or heterozygote mutations in *Wtx* seemed to affect the trabecular bone architecture. $Wtx^{floxΔ}$ male mice showed reduced trabecular separation and increased trabecular number compared to controls. In addition, bone trabeculae in $Wtx^{floxΔ}$ mice were more "plate-like," as revealed by the reduced structure model index, thus suggesting changes in trabecular orientation. Similar though less marked trends were observed for these parameters in $Wtx^{KO/+}$ female mice. Taken together, these analyses suggest that genetic inactivation of *Wtx* resulted in an increase in bone mass, which was more evident in males.

Discussion

OSCS is an X-linked disease characterized by a wide variety of skeletal defects due to germline mutations in *WTX*. The clinical symptoms vary greatly among female patients most likely due to

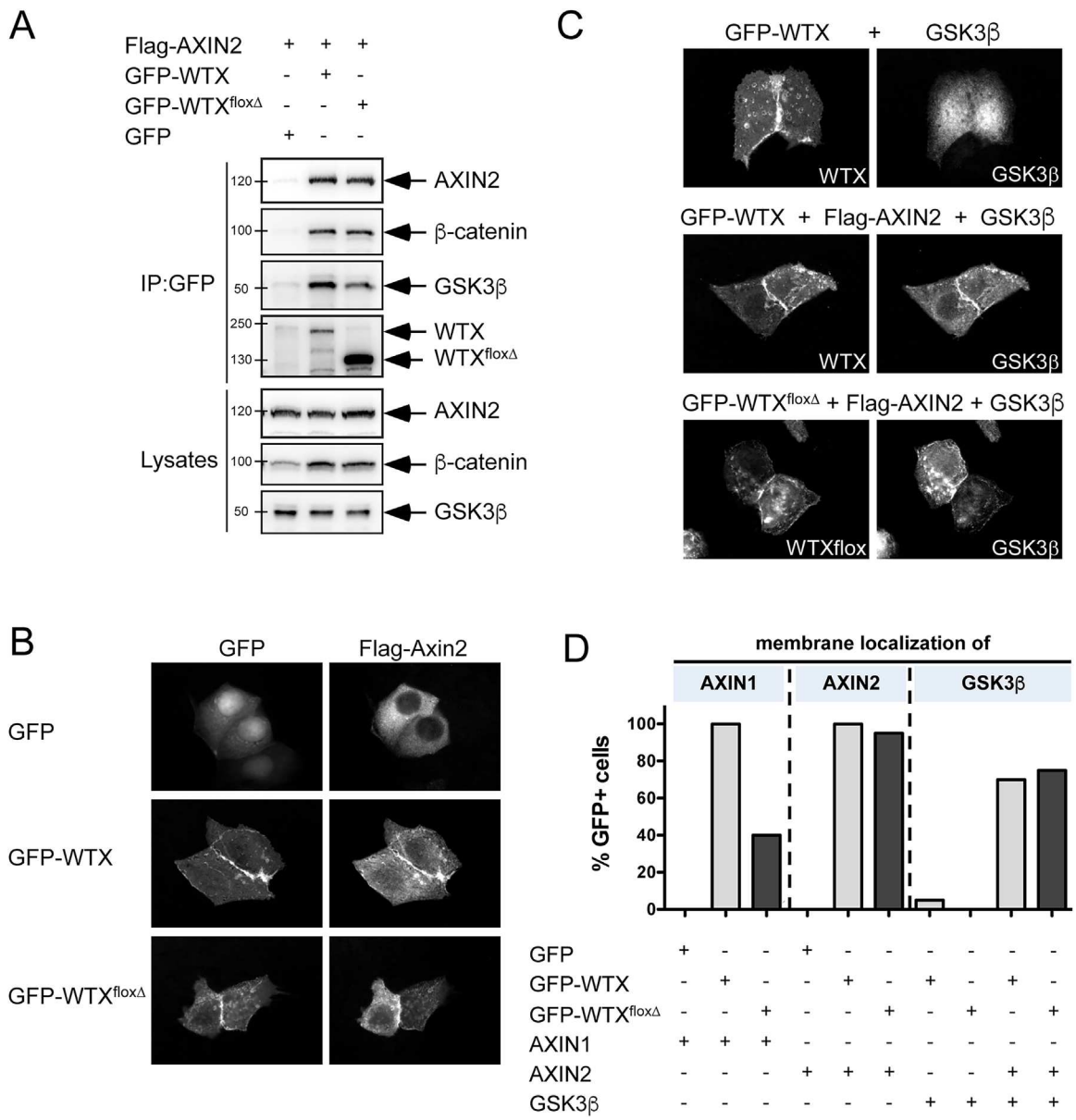

Fig. 4. WTX^{floxΔ} interacts indirectly with β-catenin. (*A*) WTX^{floxΔ} interacts with coexpressed AXIN2 in HEK293 cells. Endogenous β-catenin and GSK3β also co-immunoprecipitate with WTX^{floxΔ} in the presence of AXIN2. (*B*) WTX^{floxΔ} recruits AXIN2 from the cytoplasm to the plasma membrane. Co-transfection of GFP-WTX or GFP-WTX^{floxΔ} (left panels, GFP fluorescence) together with Flag-AXIN2 (right panels, anti-Flag immunofluorescence) in MCF-7 cells. (*C*) WTX^{floxΔ} recruits GSK3 β from its diffuse cytoplasmic localization to the plasma membrane when AXIN2 is present. MCF-7 cells were cotransfected as indicated above the panels. GFP, GFP-WTX, and GFP-WTX^{floxΔ} proteins were detected by GFP fluorescence (left panels) and GSK3β by anti-GSK3 immunofluorescence (right panels). (*D*) MCF-7 cells were cotransfected as indicated below the bars. Quantification of the percentage of transfected GFP+ cells showing membrane localization of AXIN1, AXIN2, or GSK3β. Results are from one experiment scoring at least 20 cells using the 40× objective, and are representative of three independent experiments with similar phenotypes.

variability in the ratio of random X-inactivation of the remaining wild-type *WTX* allele. In addition to this epigenetic variability, the phenotype appears to be also influenced by the type of mutation within *WTX*. Whereas gene deletions or nonsense mutations at the 5′ end of the gene are almost always lethal in male patients, truncations that affect the 3′ end generally have a less severe phenotype permitting survival till adulthood,[14,17] although it should be noted that this genotype-phenotype relationship is not absolute.[15,32] The mutant alleles generated in the present study provide us with important additional functional information, both on the developmental and molecular level.

A defining feature of the mutant phenotype in *Wtx*^{KO} mice appears to be the midline defects including severe abnormalities in the sternum, vertebrae, and the palate. Although several of these phenotypes have been reported in a previous study,[19] our analysis revealed additional defects in skull bone architecture including cleft palate and abnormal development of the base of the skull. Palatogenesis, the developmental process that forms the intact roof of the oral cavity, is often disrupted by

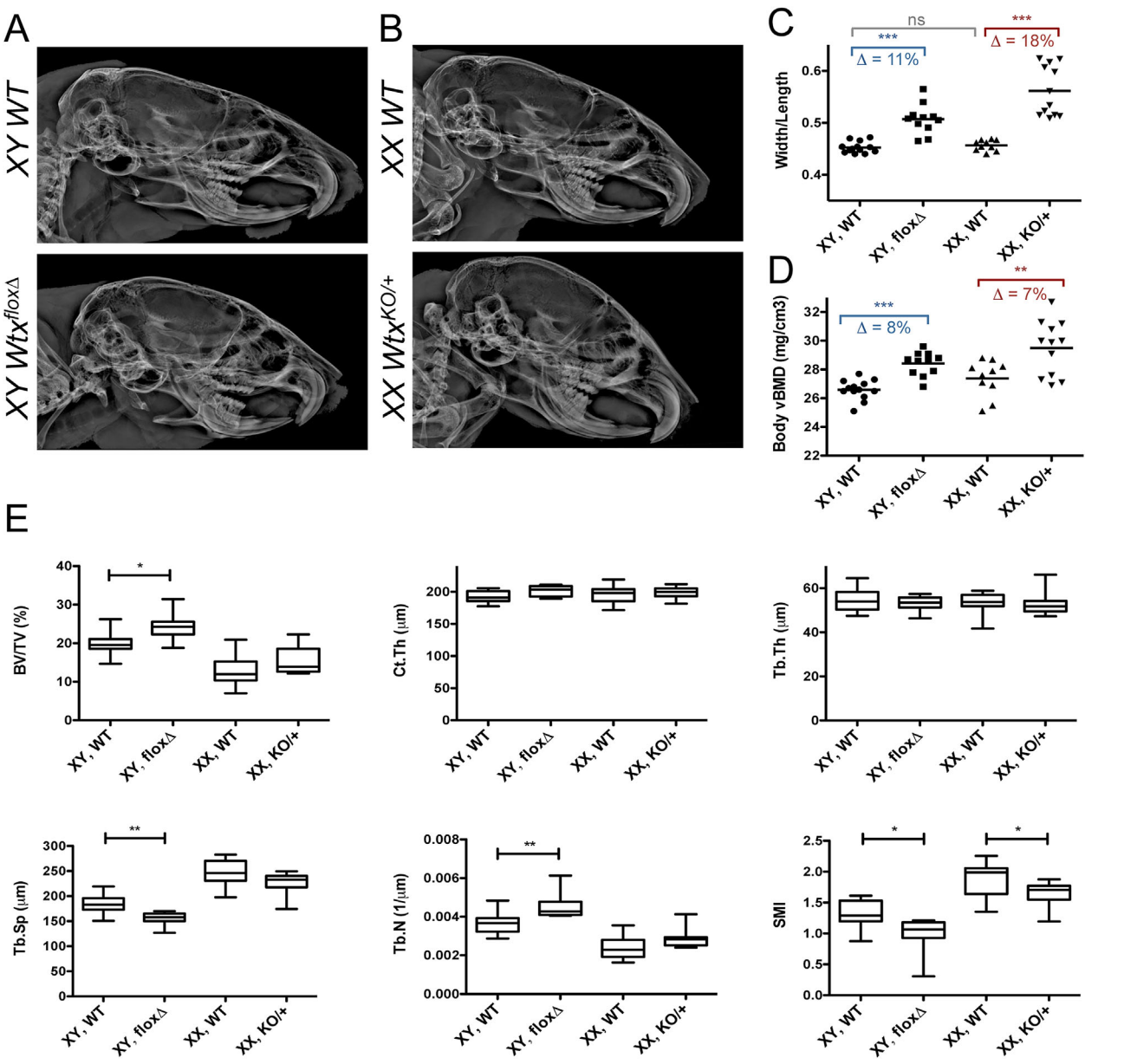

Fig. 5. Elevated BMD in *Wtx* mutant mice. (*A*, *B*) Radiographs from adult skulls showing altered skull proportions in female and male *Wtx* mutant mice. (*C*) Quantitation of skull morphometry from measurements on radiographs (see also Supplementary Fig. 5B). (*D*) Scatter plot showing the distribution (and mean) of vBMD of adult female and male WTX mutants. (*E*) μCT analysis of femurs. Whiskers represent the 5th and the 95th percentile. *n* value ≥7 for all genotypes. Student's *t* test: $^{*}p < 0.05$; $^{**}p < 0.01$; $^{***}p < 0.001$. BV/TV = bone volume/tissue volume; Ct.Th = cortical thickness; Tb.Th = trabecular thickness; Tb.Sp = trabecular separation; Tb.N = trabecular number; SMI = structure model index; vBMD = volumetric BMD.

genetic and environmental perturbations, as reflected in the high frequency of cleft palate in humans.[33] Because cleft palates are incompatible with the postnatal survival of mice, this phenotype is a likely cause of the observed perinatal lethality in male *Wtx* knockout animals. Of note, complete cleft palate was observed in only 43% of the male Wtx^{KO} analyzed, and the severity of clefting seemed to be influenced by the genetic background of the mice (increased penetrance of the full cleft when the line was in a C57BL/6 background compared to a 129SV background), an observation previously documented for other mutations.[34]

Previous studies have already demonstrated that β-catenin must be tightly regulated to permit normal palate development and both loss-of-function and gain-of-function experiments in the palatal epithelia result in failure of palatal shelf fusion.[35,36] WTX exerts its negative regulatory role in WNT signaling by interacting with key components of the β-catenin destruction complex, including APC, AXIN proteins, β-catenin, and GSK3β.[8,9] Interestingly, targeted disruption of *Gsk3β*, an important kinase targeting β-catenin for destruction, also causes cleft palate and sternal fusion defects.[37,38] Although GSK3β is considered a promiscuous kinase that can affect a wide variety of other pathways,[39] the similar phenotype with *Wtx* mutants and the fact that WTX is required for the recruitment of GSK3β to the membrane via the interaction with AXIN1 or AXIN2[10] (and this study) would argue that WTX is essential for

GSK3β to exert its function in vivo in a β-catenin–dependent context. It raises also the interesting possibility that GSK3β would require membrane localization for its function during skeletal development. Interestingly, at least at the palatal level, inactivation of *Gsk3β* does not seem to affect WNT/β-catenin reporter activity despite being expressed primarily in epithelial layers overlapping with β-catenin.[38] Therefore, the mechanistic role of GSK3β in this context remains unclear. Similarly, given that WTX can function in either the canonical WNT signaling pathway[9] or as a component of adherens junctions together with β-catenin,[7] further studies will be required to understand the precise cellular role of these proteins in palatal development.

Apart from the palatal abnormalities, we also noticed a hole in the middle or posterior region of the basisphenoid bone. A similar phenotype in the basisphenoid bone has been reported in a number of mutant mice,[40–43] including components of the WNT signaling pathway.[27,44] In addition, we also observed an ectopic ossified bridge connecting the basioccipital with the basisphenoid bone at the base of the skull at the level of the spheno-occipital synchondrosis. In the cranial base synchondroses, ie, the sutures between the bones of the skull base that serve as endochondral growth sites, a fine balance between proliferation and differentiation of chondrocytes takes place that allows embryonic and postnatal growth of the skull.[45,46] A phenotype characterized by shortened, dome-shaped skulls has been described previously for other mutants[27,45,47–49] and related to the presence of a bony bridge at this level. Because experimentally induced fusion of the base of the skull causes craniofacial shortening,[50] it is likely that ectopic synostosis is also responsible for the skull dysmorphisms observed in Wtx^{KO} mice. Importantly, the craniofacial phenotype in Wtx^{KO} and $Wtx^{flox\Delta}$ mice strongly correlates with the dysmorphism seen in OSCS patients that often display cleft palate, macrocephaly, and frontal or occipital bossing of the skull.[14,15,17] To our knowledge, the presence of bony bridges at the base of the skull has not been reported in OSCS patients, but in the light of our results it may be worth to revisit this possibility.

In addition to our Wtx^{KO} loss-of-function model that results in perinatal lethality, we also described here a less severely affected $Wtx^{flox\Delta}$ allele that produces a truncated version of the WTX protein. Human patients with truncation mutations at a comparable position also survive and show a range of skeletal anomalies that are highly similar to those found in our mouse model including macrocephaly, frontal bossing, high arched and cleft palate, and severe bone sclerosis.[14,15,17] The overlapping, but less severe phenotype of $Wtx^{flox\Delta}$ mice, when compared to the loss-of-function allele (XY Wtx^{KO}) during development, is in agreement with the truncated protein acting as a hypomorph, a hypothesis that has already been put forward for human truncation mutations[14] and is further supported by our in vitro studies.

When compared to the Wtx^{KO} allele, the developmental defects in $Wtx^{flox\Delta}$ mutants are relatively mild despite the fact that the truncated protein no longer co-immunoprecipitates with β-catenin. The C-terminal domain of WTX contains repeated arginine-glutamic acid-alanine (REA) motifs that are important for direct interaction with β-catenin.[10] This motif lies outside the conserved blocks of sequences identified in all WTX orthologues[24] and does not appear to be highly conserved throughout evolution. It is, therefore, likely that mammals have adopted the REA motif to increase the affinity of WTX to β-catenin.[10] The less severe phenotype of the $Wtx^{flox\Delta}$ mutant mice during development could be explained by an indirect interaction of the truncated protein with β-catenin via AXIN1 and AXIN2 thus retaining a certain degree of WTX function. However, the increased BMD phenotype observed in $Wtx^{flox\Delta}$ adult mice suggests that this association is inefficient and that the C-terminal domain of WTX is required to fine-tune WNT signaling. Confirming this model in vivo is, however, difficult, as the low amounts of protein do not allow efficient co-precipitation.

The fact that reducing β-catenin levels rescues to a certain extent the *Wtx* full knockout phenotype in mice[19] (our data) strongly argues that also in vivo one of the primary functions of WTX is to diminish the protein levels of this gene. However, as mentioned before, WTX has been shown to also stabilize adherens junctions in epithelial cell lines in vitro, probably by recruiting APC to the membrane.[7] Thus, it is currently unclear whether the rescue is strictly due to the re-establishment of appropriate levels of WNT/β-catenin signaling or caused by other coincident effects exerted by WTX and β-catenin at the plasma membrane. In addition, given that those *WTX* truncation mutations that retain at least one APC binding domain and membrane binding capability result in a milder phenotype (as in our $Wtx^{flox\Delta}$ allele), the membrane localization of WTX was suggested to be protective against the disease.[14] Therefore, analysis of changes in the stability of cell adhesions and levels of transcriptionally active β-catenin might help understanding the relevance of these different functions of WTX in different cellular contexts.

Bone mass is regulated by a tight balance between the activities of bone-forming osteoblasts and bone-resorbing osteoclasts. Osteocytes, ie, terminally differentiated osteoblasts embedded in the mineralized bone matrix, maintain bones and coordinate the action of osteoblasts and osteoclasts during bone modeling and remodeling.[51] The sclerosing aspect of several bones is the most prominent feature of OSCS. Therefore, we performed DXA and μCT analysis in adult Wtx^{flox} males and $Wtx^{KO/+}$ heterozygous females, because they survived beyond birth. Similarly to the human condition, we observed a significant, although milder increase in vBMD in adult $Wtx^{flox\Delta}$ male and $Wtx^{KO/+}$ female mice. A key feature for OSCS is that sclerosis is accompanied by linear striations in the metaphyseal region of the long bones of female patients.[14,16] Male patients generally do not show metaphyseal striations, with the exceptions of those carrying a mosaic mutation.[17] Although at present there is no proven explanation for the origin of the striations, variation in bone formation rate due to nonrandom X inactivation was proposed as a potential mechanism for the phenotype.[52,53] Interestingly, osteopathia striata also occurs in patients with focal dermal hypoplasia resulting from mutations in the X-linked gene *PORCN*, an enzyme required for WNT protein modification and secretion.[54] However, in contrast to the human condition, *Wtx* mouse mutants do not show striations of the long bones in adulthood up to 4 months of age[19] (and this study). This may suggest that changes in bone density caused by *Wtx* or *Porcn* mutations are less severe in mice than in men and thus not detectable by X-ray analysis. Alternatively, the spatial pattern of X-inactivation in bone progenitors during development might differ between human and mice.

A large number of studies have demonstrated that sustained WNT signaling, in particular the canonical WNT pathway, induces an overall increase in bone mass. The hyperostotic phenotypes caused by sustained β-catenin activity have been variably attributed to different cellular mechanisms: enhanced commitment toward the osteoblastic lineage, increased osteoblast activity, and inhibition of osteoclast differentiation (reviewed by Baron and Kneissel[51] and Monroe and

colleagues[55]). However, the relative impact on bone formation and resorption seems to depend on the developmental context and timing of activation of canonical WNT signaling in the different models. A previous report has provided compelling evidence that the bone overgrowth phenotype in *Wtx* mutants is at least partly due to an increased commitment of mesenchymal progenitors to the osteoblast lineage followed by a subsequent delay in the terminal differentiation of committed osteoblasts.[19] Although we have not analyzed the dynamics of bone mesenchymal progenitors during development in our mutant mice, our μCT analysis has also revealed a moderate increase in the bone volume fraction in the femur of adult $Wtx^{flox\Delta}$ male mice. Interestingly, our analysis revealed no change of cortical or trabecular thickness, which would suggest normal bone formation in our mutant animals. By contrast, we observed a significant reduction of trabecular spacing in our μCT analysis of $Wtx^{flox\Delta}$ male mice. An increase in the trabecular number in combination with reduced trabecular spacing is indicative for a decreased osteoclast activity. This may suggest that the increased bone mass in our mutants is due to decreased bone resorption rather than increased bone formation. Although the reasons for the discrepancies with the previous report[19] are unclear, it is worth mentioning the inherent differences of both analyses. Moisan and colleagues[19] analyzed 6-week-old male mice in which *Wtx* had been inactivated in skeletal mesenchymal cells (using the *Prx1-Cre* line) or in osteoblast precursors (*Osterix-Cre* line). β-catenin signaling is known to regulate the coupling of osteoblasts with osteoclast precursors, by controlling expression of osteoprotegerin (Opg), a competitive inhibitor of Rankl and Rank interaction.[55] Although the inactivation of *Wtx* in osteoblasts did not seem to affect osteoclast activity or numbers, the cell autonomous role of *Wtx* in osteoclasts, which derive from the hematopoietic lineage,[56] has not been addressed. Conversely, in our study, we analyzed germline *Wtx* mutations in 14-week-old mice (*Wtx* truncation mutation in male or heterozygote mutation in female mice), which may impact simultaneously on both osteoblast and osteoclast biology. It will therefore be interesting to perform osteoclast-specific deletion of *Wtx* to address a potential direct role of *Wtx* in regulating the differentiation and function of this cell type. Finally, sex- and age-dependent changes in bone microarchitecture,[57] as well as differences in the genetic background[58] could contribute to differences in the two models. Importantly, neither of the available *Wtx* mutant mouse models[19] (this study) fully phenocopied a β-catenin gain-of-function mutation or mutations on other negative regulators of the WNT/ β-catenin pathway.[51,55] This probably reflects the complex fine tuning of the WNT regulatory network and highlights potential β-catenin independent and stage-specific functions of WTX as suggested previously.[19]

In summary, we describe here two novel WTX alleles that vary in severity, ranging from a milder survivable form ($Wtx^{flox\Delta}$) in males to a severe and perinatal lethal one (Wtx^{KO}). Our novel $Wtx^{flox\Delta}$ allele constitutes a mouse model for OSCS that largely recapitulates the phenotype found in patients carrying truncation mutations. Thus, this strain will be a useful model to further study the molecular and cellular mechanisms leading to the phenotype and to test whether osteosclerosis can be ameliorated through therapeutic approaches.

Disclosures

All authors state that they have no conflicts of interest.

Acknowledgments

This work was supported by grants from ARC (grant 1130) and the Association for International Cancer Research (AICR grant 09-0752) to AS and by the German Federal Ministry of Education and Research (Infrafrontier grant 01KX1012) to MHdA. JB and KT were supported by a grant from the Deutsche Forschungsgemeinschaft BE1550/6-1 to JB. AB and GC were supported by ARC (French agency for cancer research) and a Marie-Curie fellowship. We thank Sebastien Schaub for assistance in confocal microscopy and Morgane Bourmaud for μCT scans. We are grateful to Marie-Christine Chaboissier and Anne-Amandine Chassot for providing mice and helpful discussions. We thank A. Kikuchi for the pcDNA-Flag-Axin1 construct and Dr Holger Scholz (Charité-Universitätsmedizin, Berlin) for the plasmid containing human WT1 cDNA.

Authors' roles: Study design: GC and AS. Data collection and analysis: GC, AB, KT, ASR, FM, AC, CP, and FJM. RB and WH performed X-ray/DXA analysis. MCS and TFB performed CT scans. Data interpretation: GC, CH, JB, MCS, and AS. Drafting manuscript: AS and GC. Approving final version of manuscript: all authors. AS takes responsibility for the integrity of the data analysis.

References

1. MacDonald BT, Tamai K, He X. Wnt/beta-catenin signaling: components, mechanisms, and diseases. Dev Cell. 2009;17(1):9–26.
2. Clevers H. Wnt/beta-catenin signaling in development and disease. Cell. 2006;127(3):469–80.
3. Angers S, Moon RT. Proximal events in Wnt signal transduction. Nat Rev Mol Cell Biol. 2009;10(7):468–77.
4. Reya T, Clevers H. Wnt signalling in stem cells and cancer. Nature. 2005;434(7035):843–50.
5. Huff V. Wilms' tumours: about tumour suppressor genes, an oncogene and a chameleon gene. Nat Rev Cancer. 2011;11(2):111–21.
6. Rivera MN, Kim WJ, Wells J, et al. An X chromosome gene, WTX, is commonly inactivated in Wilms tumor. Science. 2007;315(5812):642–5.
7. Grohmann A, Tanneberger K, Alzner A, Schneikert J, Behrens J. AMER1 regulates the distribution of the tumor suppressor APC between microtubules and the plasma membrane. J Cell Sci. 2007; 120(Pt 21): 3738–47.
8. Tanneberger K, Pfister AS, Kriz V, Bryja V, Schambony A, Behrens J. Structural and functional characterization of the Wnt inhibitor APC membrane recruitment 1 (Amer1). J Biol Chem. 2011;286(22):19204–14.
9. Major MB, Camp ND, Berndt JD, et al. Wilms tumor suppressor WTX negatively regulates WNT/beta-catenin signaling. Science. 2007;316(5827):1043–6.
10. Tanneberger K, Pfister AS, Brauburger K, et al. Amer1/WTX couples Wnt-induced formation of PtdIns(4, 5)P2 to LRP6 phosphorylation. EMBO.J. 2011;30(8):1433–43.
11. Zhang Z, Akyildiz S, Xiao Y, et al. Structures of the APC-ARM domain in complexes with discrete Amer1/WTX fragments reveal that it uses a consensus mode to recognize its binding partners. Cell Discov. 2015;1:15016.
12. Rivera MN, Kim WJ, Wells J, et al. The tumor suppressor WTX shuttles to the nucleus and modulates WT1 activity. Proc Natl Acad Sci U S.A. 2009;106(20):8338–43.
13. Kim WJ, Rivera MN, Coffman EJ, Haber DA. The WTX tumor suppressor enhances p53 acetylation by CBP/p300. Mol Cell. 2012;45(5):587–97.
14. Jenkins ZA, van Kogelenberg M, Morgan T, et al. Germline mutations in WTX cause a sclerosing skeletal dysplasia but do not predispose to tumorigenesis. Nat Genet. 2009;41(1):95–100.
15. Perdu B, de Freitas F, Frints SG, et al. Osteopathia striata with cranial sclerosis owing to WTX gene defect. J Bone Miner Res. 2010;25(1): 82–90.

16. Pellegrino JE, McDonald-McGinn DM, Schneider A, Markowitz RI, Zackai EH. Further clinical delineation and increased morbidity in males with osteopathia striata with cranial sclerosis: an X-linked disorder? Am J Med Genet. 1997;70(2):159–65.
17. Holman SK, Daniel P, Jenkins ZA, et al. The male phenotype in osteopathia striata congenita with cranial sclerosis. Am J Med Genet A. 2011; 155A(10): 2397–408.
18. Hartmann C. A Wnt canon orchestrating osteoblastogenesis. Trends Cell Biol. 2006;16(3):151–8.
19. Moisan A, Rivera MN, Lotinun S, et al. The WTX tumor suppressor regulates mesenchymal progenitor cell fate specification. Dev Cell. 2011;20(5):583–96.
20. Nagy A, Rossant J, Nagy R, Abramow-Newerly W, Roder JC. Derivation of completely cell culture-derived mice from early-passage embryonic stem cells. Proc Natl Acad Sci U S A. 1993;90(18):8424–8.
21. Schwenk F, Baron U, Rajewsky K. A cre-transgenic mouse strain for the ubiquitous deletion of loxP-flanked gene segments including deletion in germ cells. Nucleic Acids Res. 1995;23(24):5080–1.
22. Hayashi S, Lewis P, Pevny L, McMahon AP. Efficient gene modulation in mouse epiblast using a Sox2Cre transgenic mouse strain. Gene Expr Patterns. 2002; 2(1-2): 93–7.
23. Brault V, Moore R, Kutsch S, et al. Inactivation of the beta-catenin gene by Wnt1-Cre-mediated deletion results in dramatic brain malformation and failure of craniofacial development. Development. 2001;128(8):1253–64.
24. Boutet A, Comai G, Schedl A. The WTX/AMER1 gene family: evolution, signature and function. BMC Evol Biol. 2010;10:280.
25. Behrens J, Jerchow BA, Wurtele M, et al. Functional interaction of an axin homolog, conductin, with beta-catenin, APC, and GSK3beta. Science. 1998;280(5363):596–9.
26. McLeod MJ. Differential staining of cartilage and bone in whole mouse fetuses by Alcian blue and Alizarin red S. Teratology. 1980;22(3):299–301.
27. Lyashenko N, Weissenbock M, Sharir A, Erben RG, Minami Y, Hartmann C. Mice lacking the orphan receptor ror1 have distinct skeletal abnormalities and are growth retarded. Dev Dyn. 2010;239 (8):2266–77.
28. Carter DR, Bouxsein ML, Marcus R. New approaches for interpreting projected bone densitometry data. J Bone Miner Res. 1992;7(2):137–45.
29. Bouxsein ML, Boyd SK, Christiansen BA, Guldberg RE, Jepsen KJ, Muller R. Guidelines for assessment of bone microstructure in rodents using micro-computed tomography. J Bone Miner Res. 2010;25(7):1468–86.
30. Comai G, Boutet A, Neirijnck Y, Schedl A. Expression patterns of the Wtx/Amer gene family during mouse embryonic development. Dev Dyn. 2010;239(6):1867–78.
31. Fagotto F, Jho E, Zeng L, et al. Domains of axin involved in protein-protein interactions, Wnt pathway inhibition, and intracellular localization. J Cell Biol. 1999;145(4):741–56.
32. Perdu B, Lakeman P, Mortier G, Koenig R, Lachmeijer AM, Van Hul W. Two novel WTX mutations underscore the unpredictability of male survival in osteopathia striata with cranial sclerosis. Clin Genet. 2011;80(4):383–8.
33. Bush JO, Jiang R. Palatogenesis: morphogenetic and molecular mechanisms of secondary palate development. Development. 2012;139(2):231–43.
34. Proetzel G, Pawlowski SA, Wiles MV, et al. Transforming growth factor-beta 3 is required for secondary palate fusion. Nat Genet. 1995;11(4):409–14.
35. Funato N, Nakamura M, Yanagisawa H. Molecular basis of cleft palates in mice. World J Biol Chem. 2015;6(3):121–38.
36. He F, Xiong W, Wang Y, et al. Epithelial Wnt/beta-catenin signaling regulates palatal shelf fusion through regulation of Tgfbeta3 expression. Dev Biol. 2011;350(2):511–9.
37. Liu KJ, Arron JR, Stankunas K, Crabtree GR, Longaker MT. Chemical rescue of cleft palate and midline defects in conditional GSK-3beta mice. Nature. 2007;446(7131):79–82.
38. He F, Popkie AP, Xiong W, et al. Gsk3beta is required in the epithelium for palatal elevation in mice. Dev Dyn. 2010;239(12):3235–46.
39. Frame S, Cohen P. GSK3 takes centre stage more than 20 years after its discovery. Biochem J. 2001;359(Pt 1):1–16.
40. Baffi MO, Slattery E, Sohn P, Moses HL, Chytil A, Serra R. Conditional deletion of the TGF-beta type II receptor in Col2a expressing cells results in defects in the axial skeleton without alterations in chondrocyte differentiation or embryonic development of long bones. Dev Biol. 2004;276(1):124–42.
41. Jena N, Martin-Seisdedos C, McCue P, Croce CM. BMP7 null mutation in mice: developmental defects in skeleton, kidney, and eye. Exp Cell Res. 1997;230(1):28–37.
42. Holst CR, Bou-Reslan H, Gore BB, et al. Secreted sulfatases Sulf1 and Sulf2 have overlapping yet essential roles in mouse neonatal survival. PLoS One. 2007;2(6): e 575.
43. Bose J, Grotewold L, Ruther U. Pallister-Hall syndrome phenotype in mice mutant for Gli3. Hum Mol Genet. 2002;11(9):1129–35.
44. Brugmann SA, Goodnough LH, Gregorieff A, et al. Wnt signaling mediates regional specification in the vertebrate face. Development. 2007;134(18):3283–95.
45. Kolpakova-Hart E, McBratney-Owen B, Hou B, et al. Growth of cranial synchondroses and sutures requires polycystin-1. Dev Biol. 2008;321(2):407–19.
46. McBratney-Owen B, Iseki S, Bamforth SD, Olsen BR, Morriss-Kay GM. Development and tissue origins of the mammalian cranial base. Dev Biol. 2008;322(1):121–32.
47. Eswarakumar VP, Monsonego-Ornan E, Pines M, Antonopoulou I, Morriss-Kay GM, Lonai P. The IIIc alternative of Fgfr2 is a positive regulator of bone formation. Development. 2002;129(16): 3783–93.
48. Dabovic B, Chen Y, Colarossi C, et al. Bone abnormalities in latent TGF-[beta] binding protein (Ltbp)-3-null mice indicate a role for Ltbp-3 in modulating TGF-[beta] bioavailability. J Cell Biol. 2002;156(2):227–32.
49. Dabovic B, Chen Y, Colarossi C, Zambuto L, Obata H, Rifkin DB. Bone defects in latent TGF-beta binding protein (Ltbp)-3 null mice; a role for Ltbp in TGF-beta presentation. J Endocrinol. 2002;175(1):129–41.
50. Rosenberg P, Arlis HR, Haworth RD, Heier L, Hoffman L, LaTrenta G. The role of the cranial base in facial growth: experimental craniofacial synostosis in the rabbit. Plast Reconstr Surg. 1997;99(5):1396–407.
51. Baron R, Kneissel M. WNT signaling in bone homeostasis and disease: from human mutations to treatments. Nat Med. 2013;19(2):179–92.
52. Viot G, Lacombe D, David A, et al. Osteopathia striata cranial sclerosis: non-random X-inactivation suggestive of X-linked dominant inheritance. Am J Med Genet. 2002;107(1):1–4.
53. Kraus C, Konig R, Rott HD. Comments on "osteopathia striata cranial sclerosis: non-random X-inactivation suggestive of X-linked dominant inheritance". Am J Med Genet A. 2003;119A(3):400.
54. Vreeburg M, van Geel M, van den Heuij LG, Steijlen PM, van Steensel MA. Focal dermal hypoplasia in a male patient due to mosaicism for a novel PORCN single nucleotide deletion. J Eur Acad Dermatol Venereol. 2011;25(5):592–5.
55. Monroe DG, McGee-Lawrence ME, Oursler MJ, Westendorf JJ. Update on Wnt signaling in bone cell biology and bone disease. Gene. 2012;492(1):1–18.
56. Crockett JC, Rogers MJ, Coxon FP, Hocking LJ, Helfrich MH. Bone remodelling at a glance. J Cell Sci. 2011; 124(Pt 7): 991–8.
57. Glatt V, Canalis E, Stadmeyer L, Bouxsein ML. Age-related changes in trabecular architecture differ in female and male C57BL/6J mice. J Bone Miner Res. 2007;22(8):1197–207.
58. Syberg S, Petersen S, Beck Jensen JE, et al. Genetic background strongly influences the bone phenotype of P2 $\times$ 7 receptor knockout mice. J Osteoporos. 2012;2012:391097.
59. Vanhoutteghem A, Maciejewski-Duval A, Bouche C, et al. Basonuclin 2 has a function in the multiplication of embryonic craniofacial mesenchymal cells and is orthologous to disco proteins. Proc Natl Acad Sci U S A. 2009;106(34):14432–7.